THE JOURNAL OF PHYSICAL CHEMISTRY B

Article

pubs.acs.org/JPCB

Observing Solvation Dynamics with Simultaneous Femtosecond X-ray Emission Spectroscopy and X-ray Scattering

Kristoffer Haldrup,[†] Wojciech Gawelda,[*,‡] Rafael Abela,[◆] Roberto Alonso-Mori,[▽] Uwe Bergmann,[▽] Amélie Bordage,[⊥,¶] Marco Cammarata,[▽,∞] Sophie E. Canton,[#] Asmus O. Dohn,[∥] Tim Brandt van Driel,[†] David M. Fritz,[▽] Andreas Galler,[‡] Pieter Glatzel,[○] Tobias Harlang,[#] Kasper S. Kjær,[†,#] Henrik T. Lemke,[▽,◆] Klaus B. Møller,[∥] Zoltán Németh,[⊥] Mátyás Pápai,[⊥,∥] Norbert Sas,[⊥] Jens Uhlig,[#] Diling Zhu,[▽] György Vankó,[⊥] Villy Sundström,[#] Martin M. Nielsen,[†] and Christian Bressler[‡,§]

[†]Department of Physics, Technical University of Denmark, Fysikvej 307, DK-2800 Kongens Lyngby, Denmark

[‡]European XFEL GmbH, Albert-Einstein-Ring 19, D-22761 Hamburg, Germany

[§]The Hamburg Center for Ultrafast Imaging, Universität Hamburg, Luruper Chaussee 149, D-22761 Hamburg, Germany

[∥]Department of Chemistry, Technical University of Denmark, Kemitorvet 207, DK-2800 Kongens Lyngby, Denmark

[⊥]Wigner Research Centre for Physics, Hungarian Academy Sciences, H-1525 Budapest, Hungary

[#]Department of Chemical Physics, Lund University, Box 118, S-22100 Lund, Sweden

[▽]LCLS, SLAC National Accelerator Laboratory, Menlo Park, California 94025, United States

[○]European Synchrotron Radiation Facility, F-38043 Grenoble Cedex 9, France

[◆]Paul Scherrer Institut, SwissFEL, CH-5232 Villigen PSI, Switzerland

Supporting Information

ABSTRACT: In liquid phase chemistry dynamic solute−solvent interactions often govern the path, ultimate outcome, and efficiency of chemical reactions. These steps involve many-body movements on subpicosecond time scales and thus ultrafast structural tools capable of capturing both intramolecular electronic and structural changes, and local solvent structural changes are desired. We have studied the intra- and intermolecular dynamics of a model chromophore, aqueous $[Fe(bpy)_3]^{2+}$, with complementary X-ray tools in a single experiment exploiting intense XFEL radiation as a probe. We monitored the ultrafast structural rearrangement of the solute with X-ray emission spectroscopy, thus establishing time zero for the ensuing X-ray diffuse scattering analysis. The simultaneously recorded X-ray diffuse scattering patterns reveal slower subpicosecond dynamics triggered by the intramolecular structural dynamics of the photoexcited solute. By simultaneous combination of both methods only, we can extract new information about the solvation dynamic processes unfolding during the first picosecond (ps). The measured bulk solvent density increase of 0.2% indicates a dramatic change of the solvation shell around each photoexcited solute, confirming previous ab initio molecular dynamics simulations. Structural changes in the aqueous solvent associated with density and temperature changes occur with ∼1 ps time constants, characteristic for structural dynamics in water. This slower time scale of the solvent response allows us to directly observe the structure of the excited solute molecules well before the solvent contributions become dominant.

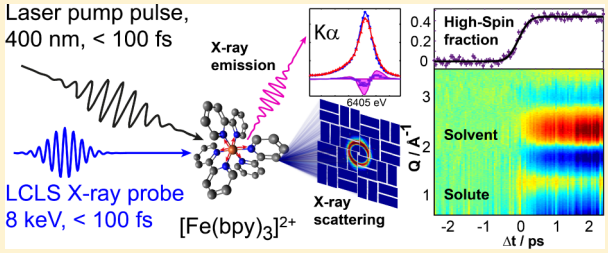

1. INTRODUCTION

Solvation dynamics, the process of solvent shell reorganization upon electronic or structural changes in a solute, is one of the most studied phenomena in physical chemistry.[1] However, it has evaded direct observation on the molecular level due to the involved many-body dynamics and concomitant fast, subpicosecond, intramolecular dynamics, until recent advances in time-resolved X-ray science became available.[2,3] A vast majority of photochemical reactions proceed via electronically excited states, which involve an ultrafast redistribution of the ground state charges. This consequently modifies the intra-atomic potential energy surfaces within the system, which may drive subsequent bond-breaking and -making or other structural transformations.[4] The nonequilibrium electronic charge distribution will also have a significant impact on the forces experienced between the solute and solvent molecules, causing the latter to rearrange and adjust to the new solute electronic and structural configuration. As a consequence, the solvent molecules surrounding the solute may not act solely as

Received: December 21, 2015
Published: January 19, 2016

DOI: 10.1021/acs.jpcb.5b12471
J. Phys. Chem. B 2016, 120, 1158−1168

spectators providing just a heat bath but can actively influence the outcome of a chemical reaction,[5] dynamically influencing both the reactant and product potential energy landscapes and thus the pathway for molecular structure changes in the transition states. Since most of chemical reactions and biological functions take place in solution, detailed knowledge of the very first steps of solvent−solute interactions on their fundamental ultrafast timescales, i.e., from femtoseconds (fs) to picoseconds (ps), is paramount toward a complete understanding of liquid-phase reactivity.

In view of the interactions taking place between solvent molecules but also within the reacting molecule itself, their combined (solvation) dynamics are inherently difficult to monitor on the molecular level. Therefore most prior studies relied on indirect evidence of the underlying dynamics, in most cases derived from a combination of nonlinear optical spectroscopies[6−11] and molecular dynamics simulations.[12−15] In consequence, it is desirable to develop new ultrafast time-resolved structural tools capable of directly resolving the electronic, spin, and geometric structure changes for both the solute and the solvent molecules simultaneously and preferably in a single experiment to leave little room for an ambiguous interpretation. The approach used here involves both X-ray emission spectroscopy (XES), which allows for studying the local electronic structure (oxidation and spin states, occupied density of states, etc.) of the selected solute molecule and *simultaneously* recorded ultrafast X-ray diffuse scattering (XDS) patterns, which can deliver information about both solute and (bulk) solvent structures. With this approach we now go beyond the sensitivity of all-optical probes and likewise exploit X-ray spectroscopies to extract electronic information about evolving optically dark states.[16,17]

In the present experiment we studied aqueous $[Fe(bpy)_3]^{2+}$. The chosen spin transition compound exhibits not only ultrafast charge transfer and back transfer processes but also a subpicosecond transition into its paramagnetic high-spin (HS) state with $\Delta S = 2$. Its reaction sequence has been studied in much detail with femtosecond-resolved optical transient absorption and fluorescence spectroscopies.[11,18] Briefly, the initial photoexcitation into the Franck−Condon ^{1}MLCT (Metal-to-Ligand Charge Transfer) manifold is followed by a prompt (<30 fs) intersystem crossing into the ^{3}MLCT manifold, as has been also observed for the isostructural complex $[Ru(bpy)_3]^{2+}$ [19] next to similar Ir-based compounds.[20,21] The dynamics of MLCT states are strongly coupled to the surrounding environment, and for $[Ru(bpy)_3]^{2+}$ both theoretical[22] and experimental[23,24] studies have revealed a profound influence of the solvent on the coordination symmetry and charge localization on the bpy ligands via nondiffusive solvation dynamics. In the case of $[Ru(bpy)_3]^{2+}$, the lowest energy ^{3}MLCT state is very reactive and has a 300 ns lifetime, which lead to charge transport and subsequent bimolecular reactions on longer timescales.[25] On the contrary, the ^{3}MLCT state of $[Fe(bpy)_3]^{2+}$ has lower energy and its 100 fs lifetime is due to a strong coupling to the manifold of underlying ligand-field (LF) states,[26] which are well-shielded from solute−solvent interactions. In this sense, the solvation dynamics of $[Fe(bpy)_3]^{2+}$ are drastically different from the case of aqueous $[Ru(bpy)_3]^{2+}$, since it does not involve extensive solvent interactions with the MLCT states. The photoabsorbed energy is instead efficiently transferred, with nearly unit quantum yield into the lowest quintet $^5T_2$ HS state, which eventually relaxes nonradiatively back to the low-spin (LS) ground state in 0.65 ns at room temperature.[27] Even at high excitation intensities (>4 TW/cm^2), no other photoproducts were observed apart from the lowest HS state, which makes this system an ideal candidate to test new experimental approaches on the ultrafast time scales.[28] This reaction cycle was previously studied with femtosecond X-ray absorption spectroscopy, which confirmed the LS → HS conversion and the concomitant 0.2 Å Fe−N bond lengthening to occur within <250 fs [29] and with internal vibrational relaxation taking place in 1−2 ps.[30] In a recent study, under similar high-intensity laser excitation conditions, by Zhang et al.[31] the coupled charge and spin dynamics of $[Fe(bpy)_3]^{2+}$ upon dynamic spin transition was studied with femtosecond-resolved XES using ultraintense and ultrashort X-ray pulses from an X-ray Free Electron Laser delivering first insights on the involvement of the intermediate MLCT and LF states during the relaxation process toward the HS state. While these prior studies revealed much information about the intramolecular dynamic processes during this spin transition process, all aspects of solute−solvent interactions occurring on the ultrafast time scales remain in the dark.

In a recent effort we set up a combined time-resolved X-ray experiment exploiting simultaneously XES and XDS on $[Fe(bpy)_3]^{2+}$ on the 100 ps time scale by utilizing MHz laser-pump/X-ray probe at a synchrotron facility.[32,33] This experiment aimed to deliver new insight in the electronic and geometric structural reorganization of solute molecules in bulk solvents, and combining structural with electronically sensitive tools proved to be a well suited experimental approach for this purpose. Although limited to 100 ps time resolution, we simultaneously followed the HS population fraction with both XES and XDS but also determined the heat dissipation into the solvent (via XDS) due to the radiationless deactivation from the HS state to the LS ground state with its characteristic lifetime of 0.6 ns. This underlines the strength of using XDS to monitor key thermodynamic properties in a reacting sample, albeit averaged over the bulk sample. Quite surprisingly, this XDS analysis also yielded an average bulk density *increase* after 100 ps, which then *decreased* in time with the same 0.6 ns time constant, which has never before been observed in TR XDS studies. The extracted density increase was quantitatively very similar to what one would expect for expelling two H_2O molecules from the caging water shell, for each excited solute molecule, into the bulk solvent (at constant volume on this 100 ps time scale). This result verified a recent ab initio molecular dynamics study of the reorganization of the solvation shell between the LS and the HS states of aqueous $[Fe(bpy)_3]^{2+}$.[34] It was concluded that upon formation of the HS state, on average two H_2O molecules are expelled from the first solvation shell around the solute, which consists of solvent molecules intercalated between the bpy ligands. The observed density decrease with the 0.6 ns HS → LS was accurately explained by the (re)inclusion of both expelled H_2O molecules, once the ground state solute structure has been re-established.

Earlier studies at XFEL sources used combined X-ray diffraction and XES techniques to study much slower processes occurring in the Mn-based reaction center of photosystem II, allowing the extraction of element-specific information about the metastable electronic structure of the metal ion and the long-range structural changes of the entire protein environment[35,36] Only recently, femtosecond XDS has been successfully applied to study protein structural dynamics using hard X-ray FEL pulses on samples excited with high-intensity laser pulses.[37,38] These studies showed that the energy

DOI: 10.1021/acs.jpcb.5b12471
J. Phys. Chem. B 2016, 120, 1158−1168

dissipation in proteins proceeds via rapid "quakelike" structural motions on timescales shorter than those for heat propagation through the protein. Using combined femtosecond-resolved XDS and XES has also been applied to investigate the ultrafast intramolecular electron transfer in a prototype photocatalytic molecular complex in solution.[39] Here the simultaneous information about the transient electronic (spin state via XES) and molecular structures of the solute and surrounding solvent, via XDS, was recorded with <2 ps temporal resolution.

Relevant for the present work a very recent femtosecond-resolved optical laser study[11] investigated the transient absorption in the UV−VIS range with remarkable sub-50 fs time resolution, indicating a faster relaxation into the HS state in conflict with a recently established via fs XES (with 150 fs time resolution).[31] However, the present work seeks to deliver a direct glimpse into solute−solvent interactions on the subpicosecond time scale with a time resolution of only 0.5 ps. With the limited time resolution we can nevertheless disentangle intra- from intermolecular dynamic processes during this LS−HS process.

Here we test the applicability of combined complementary X-ray tools for solvation dynamics on the subpicosecond time scale. It is extremely fascinating to explore their potential to actually monitor evolving chemical reactions including their complex solvation dynamics down to the fundamental time scales of a few tens of femtoseconds. This work seeks to enter this new field recently now possible with the availability of exceptionally intense and ultrashort X-ray pulses from the now worldwide emerging XFEL sources.

2. EXPERIMENTAL APPROACH

The experiments were performed at the Linac Coherent Light Source (LCLS),[40] making use of the X-ray Pump−Probe (XPP) endstation. Details of the beamline have been described in our previous femtosecond XANES experiment,[41] and the here added instrumentation is shown in Figure 1.

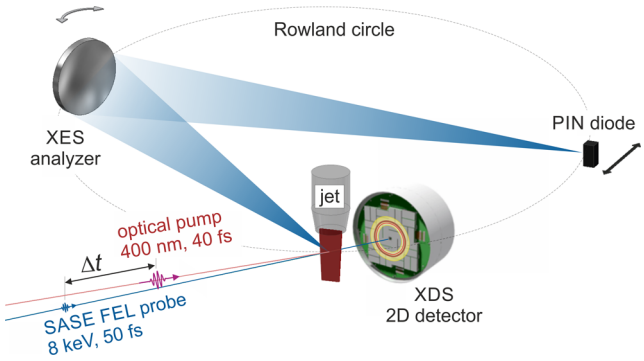

Figure 1. Schematic layout of the experimental pump−probe setup, showing the overlapping optical and X-ray laser beams on the sample. The emitted X-ray fluorescence was collected in a Rowland-circle XES setup, and forward scattered X-ray photons (XDS) were detected by the CS-PAD detector system.

The sample consisted of 50 mM of aqueous $[Fe(bpy)_3]^{2+}$ circulating through a sapphire nozzle generating a flat sheet of 0.1 mm thickness. The sample was excited at 120 Hz with 200 μJ/400 nm and 50 fs long laser pulses. SASE radiation from LCLS at 8 keV probed the sample at the same 120 Hz in the so-called pink beam mode (X-ray bandwidth 0.3%) with a nominal pulse width of <80 fs. The probe flux was around 10^{14} photons/s (10^{12} photons/pulse) on average with rather large pulse-to-pulse variations; thus normalization with respect to X-ray intensity for each shot was vital for the analysis.[41] Laser and X-ray beams were overlapped on the sample (0.15 mm laser spot diameter and 0.14 mm X-ray spot diameter), and the chosen flow speed allowed complete sample refreshment after each pump−probe measurement.

The vertically free-flowing liquid sheet was rotated to 45° to allow simultaneous detection of the X-rays scattered in forward direction and the X-ray fluorescence emitted from the beam-facing sample surface at 90°. The X-ray fluorescence was focused onto a PIN diode using a spherically bent Si (531) analyzer crystal with 1 m bending radius (see Figure 1) with an energy resolution of ∼1 eV around the Fe Kα emission lines. The entire sample-crystal-detector setup was enclosed in a He atmosphere to reduce the loss of fluorescence intensity due to absorption in air.

The XDS signal was measured in forward direction using a large-area (32 modules) CS-PAD detector[42] mounted on a robot arm downstream of the sample chamber, with a central hole permitting transmission of the intense XFEL pulses. The 2D images were recorded and stored for each pump−probe event and azimuthally integrated to yield 1D scattering curves $S(2\theta)$ with $2\theta_{max} = 60°$ corresponding to a maximum scattering vector $Q_{max} = 4$ Å^{-1}. Time scans were usually recorded in steps of 50 fs throughout the −2.5 to + 2.5 ps range, and each time step recorded 240 pump−probe events, simultaneously collecting XDS and XES data for each pump−probe shot. XES energy scans at selected (nominal) time delays were recorded in 0.5 eV steps for 240 pump−probe events each. Static data were recorded identical to the above protocol with the optical laser beam blocked and at negative pump−probe time delays. The XES data were equally normalized to the incident flux, and the XDS data were in addition calibrated and normalized against a known standard (water) (see Supporting Information for details).

Conducting simultaneous XES and XDS measurements allows us to extract dynamic information starting with the purely electronic processes affecting the photoexcited solute molecules, over the subsequent structural dynamics and the solute−solvent interactions responsible for dissipating the photoinjected excess energy. Hereby the setup allows recording of both XES signals and the XDS patterns for every pump−probe event, and the nominal time delays for both measurements are thus identical. When extracting the temporal behavior of each signal, we can thus rely on the identity on the time axis, which enables the temporal interpretation given below.

At the time of this experiment, the later developed arrival-time diagnostic tools[43] were not available. XES and XDS data were collected with a nominal step size of 50 fs, albeit knowing that there are laser/X-ray timing jitters (with 0.5 ps, see below), leading to a temporal broadening of the measured response. Important for the present work, the temporal broadening or instrument response function (IRF) is the same for XES and XDS at a given time delay, and this allows us to directly connect the extracted results from XES and XDS into one single picture as described below.

3. RESULTS AND DISCUSSION

The analysis strategy is analoguos to our previous picosecond time-resolved synchrotron study,[32] and details can be found in the Supporting Information. It relies on the input from the XES

DOI: 10.1021/acs.jpcb.5b12471
J. Phys. Chem. B 2016, 120, 1158−1168

analysis (to reliably define time zero for the XDS data) and thus to derive the solvation response with subpicosecond time resolution.

3.1. X-ray Emission Spectroscopy Analysis. Figure 2 shows the recorded Fe Kα emission spectra with and without

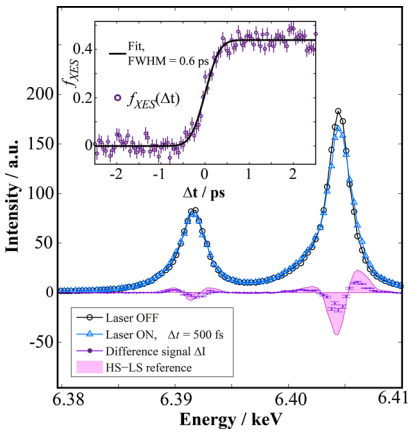

Figure 2. Measured Kα XES spectrum of $[Fe(bpy)_3]^{2+}$ is shown for both ground state (black) and the photoexcited species (blue) together with the difference spectrum (at 500 fs time delay). The static difference spectrum for LS and HS reference compounds (corresponding to a complete spin conversion) is shown for comparison. The inset graph shows the time scan (purple points) measured at the strongest peak in the Kα spectrum (~6405 eV), and the observed kinetics were fitted with a broadened step function (black line).

laser excitation of the sample (blue and black trace, respectively), and their difference signal is shown as dark purple points (area shaded as well). The Kα XES at the nominal time delay Δt = 500 fs shows distinct changes compared to the ground state, which indicate the fully completed spin state transition on this time scale. By scaling to the difference spectrum between the LS state and a separate HS reference sample (here, $[Fe(phen)_2(NCS)_2]$ and shown in the light purple area in Figure 2), we extract the HS fraction population $f_{XES}(\Delta t)$.[44,45]

The emission intensity at a single energy (here, the maximum of the $K\alpha_1$ line) can be used to accurately monitor the spin state of the absorber (see inset in Figure 2)[44] as a function of the relative time delay Δt between optical and X-ray pulses, allowing us to track the HS population kinetics. A simple 0.6 ps Gaussian broadened step function fits the observed evolution very well and allows a preliminary estimate of Δt = 0. However, here we utilize a subsequent experiment with 0.15 ps time resolution[31] under similar laser excitation conditions of aqueous $[Fe(bpy)_3]^{2+}$, which delivered for the LS → HS conversion a (roughly) exponential rise with a 0.15 ps time constant. Since neither our laser nor the X-ray pulse widths of 50 and 80 fs, respectively, are different from the previously determined rise time (but our cross correlation is 0.5 ps versus their 0.15 ps), we can safely use this exponential rise to fit the kinetics of our TR XES signal.

In consequence, even though the time evolution of $f_{XES}(\Delta t)$ is well described by a simple 0.6 ps broadened Gaussian-broadened step function, the information about the ^{3}MLCT state is established with that same time constant of 0.15 ps and allows us to apply an improved model for the observed kinetics, based on this prior knowledge (thus using the rise time τ = 0.15 ps and fitting the Gaussian IRF together with time zero of this experiment). We find time zero $t_0 = -0.14(0.08)$ ps and the IRF width of 0.5(1) ps fwhm. As the XES and XDS data were acquired truly simultaneously for each pump−probe shot, we can "lock" both values in the kinetic analysis of the XDS results (described below). This approach exploiting complementary observables in the same experiment highlights the significant advantage for the interpretation of the results given below.

3.2. X-ray Diffuse Scattering Analysis. Since the XDS data were recorded simultaneously with the XES signal, the starting point for the analysis of the XDS data is a set of difference signals at (and with now precisely known time zero (Table 1)) different time delays $\Delta S(Q,\Delta t) = S(Q,\Delta t) - S(Q)_{Off}$[46] where $S(Q)_{Off}$ refers to an average over many measurements at significantly negative time delays (here for all delays $\Delta t \leq -1.2$ ps). A subsequent step utilized singular value decomposition to identify and remove significant artifacts in the difference signals,[47] and Figure 3a shows the resulting set of 50 fs binned difference signals in matrix form, utilizing color coding to indicate the transient signal intensities.

Table 1. Kinetic Model Fit Results

fit parameter	t_0, ps	IRF, ps	τ, ps
$f_{XES}(\Delta t)$	−0.14 ± 0.08	0.5 ± 0.1	0.15[b]
$f_{XDS}(\Delta t)$	−0.06 ± 0.1[a]	0.5 ± 0.2[a]	0.6 ± 0.2
$\Delta T(\Delta t)$	−0.08 ± 0.05[a,c]	0.4 ± 0.2[a]	1.1 ± 0.2
$\Delta\rho(\Delta t)$	−0.06 ± 0.09[a,c]	0.4 ± 0.4[a,c]	1.1 ± 0.3

[a]These parameters were constrained within the XES-determined confidence intervals. [b]Set to published value, i.e. ref 31. [c]Confidence interval estimated, as one or more of the XES-determined parameter bounds were reached during the fit.

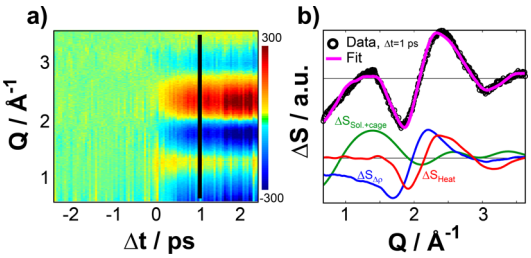

Figure 3. (a) 2D representation of XDS difference signal $\Delta S(Q,\Delta t)$, the black line indicates the difference signal shown in (b). (b) 1D difference XDS signal is shown for a time delay Δt = 1 ps (black circles) together with a corresponding best-fit model ΔS_{model} (magenta line). The bottom part of (b) displays the different components contributing to the total difference signal at this time delay (see text for details).

Figure 3b, top panel, shows a representative 1D difference XDS signal $\Delta S(Q,\Delta t$=1 ps), where the system is completely in its final HS state. In order to analyze the extracted transient XDS data, we use the methodology developed at synchrotrons over the past decade for studies with 100 ps time resolution.[32,46,48−50] In the present case, the analysis is based on representing the observed difference signal as a combination of several contributions:

$$\Delta S = \Delta S_{Sol\text{-}cage} + \Delta S_{\Delta T} + \Delta S_{\Delta\rho} \quad (1)$$

The first term $\Delta S_{Sol\text{-}cage}$ describes the difference scattering signal expected to arise from the known solute structural change, i.e., 0.2 Å metal−ligand bond expansion.[51] This contribution is

DOI: 10.1021/acs.jpcb.5b12471
J. Phys. Chem. B 2016, 120, 1158−1168

calculated via the Debye equation applied to ensembles of (classical) molecular dynamics simulations of the solute + solvent system, with the solute structures derived from ab initio molecular dynamics simulations[34] in complete analogy with our previous work.[32]

The solvent contributions $\Delta S_{\Delta T}$ and $\Delta S_{\Delta \rho}$ are determined in separate experiments as described in detail in refs 52 and 53. The $\Delta S_{\Delta T}$ term describes changes in scattering due to structural changes arising from temperature changes of the solvent via $\Delta S_{\Delta T} = \Delta T \times \partial(S(Q))/\partial T|_{\rho}$. Finally, $\Delta S_{\Delta \rho}$ describes any change in the bulk solvent density via $\Delta S_{\Delta \rho} = \Delta \rho \times \partial(S(Q))/\partial \rho|_{T}$.

The chosen methodology is based on the successful development of this treatment at synchrotron sources for experiments on timescales limited by the 100 ps pulse width at these sources, which is sufficient time for establishing thermodynamic equilibrium. We note that on the timescales of the present experiment the probed sample volume is far from thermodynamic equilibrium due to the photoexcitation by the intense femtosecond laser pump pulse. Consequently, the interpretation becomes more complex as discussed below and in the Supporting Information. Overall, the approach via equation 1 follows the prior analysis of the picosecond data, where the individual contributions are determined from reference measurements and calculated according to DFT/MD simulations, and a linear combination of these difference signals is then fitted to the experimental data to obtain their individual weights for each time step. Equation 1 is thus used to fit the difference XDS curves, as shown in the bottom part of Figure 3b, via a linear least-squares minimization of

$$\Delta S_{\mathrm{exp}} - \Delta S_{\mathrm{model}} = \Delta S_{\mathrm{exp}} - [f_{\mathrm{XDS}}\ \Delta S_{\mathrm{Sol\text{-}cage}} + \Delta T\ \partial(S(Q))/\partial T|_{\rho} + \Delta \rho\ \partial(S(Q))/\partial \rho|_{T}] \quad (2)$$

for every time delay Δt and with the fit variables being f_{XDS} denoting the fraction of photoexcited solute molecules and ΔT and $\Delta \rho$ being the temperature and density changes, respectively.

Perhaps the most salient part of the solvent response on these short time scales is the observation of a density *increase* as in our previous XDS analysis.[32] We clearly observe this effect also on the subpicosecond time scale, which lends support to our assignment of the density increase to the expulsion of approximately two caging solvent molecules into the bulk solvent, following each photoexcited solute Fe−N bond expansion.

Figure 3b shows the data and fit in the top panel and the three independent contributions to the fit in the lower panel. For clarity of presentation the second-order heating signal has been included in ΔS_{Heat} (see Supporting Information for more details). As discussed in detail below, the high laser excitation intensity utilized in these experiments causes multiphoton ionization of the solvent molecules. This process is predominantly near the entrance surface, leading to a highly anisotropic temperature profile through the 0.1 mm liquid sheet as energy is released into the solvent. As a result, this necessitates the inclusion of a second-order temperature component to fully describe the temperature-induced XDS signal arising from the significantly hotter regions in the sample, which finally delivered a satisfactory fit. From this fit we find $f_{\mathrm{XDS}}(\Delta t = 2.5\ \mathrm{ps}) = 0.41 \pm 0.02$ (40%), which is close to the value derived from the XES data with $f_{\mathrm{XES}}(\Delta t = 2.5\ \mathrm{ps}) = 0.44 \pm 0.05$ (44%). The latter is insensitive to the changes of the solvent bath, notably to both ΔT and $\Delta \rho$. It is worth pointing out that the above-mentioned contributions to $\Delta S_{\mathrm{model}}$ have all been determined completely independently from the present data, thus avoiding any bias between data and models, as can be the case in, for example, analysis of optical spectra based on decay-associated spectra. By use of this combination of contributions to model the data, very good agreement is obtained between model and data for the transient XDS as illustrated in the top part of Figure 3b.

3.3. Influence of High Laser Excitation Intensities. Utilizing such high laser excitation intensities as in the present work requires a careful examination of the possible reaction products and requires ruling out potential artifacts in the present in the data (see Supporting Information for a thorough discussion). There are the following reaction products, which may contribute to the measured XDS and XES signals right after photoexcitation (within the first picosecond): (i) multiphoton ionization of the solvent generates solvated electrons, but also multiphoton ionization of the reactant $[Fe^{II}(bpy)_3]^{2+}$ itself may generate (ii) oxidized $[Fe^{III}(bpy)_3]^{3+}$, both products appearing promptly after photoexcitation. However, the XDS signal is not significantly influenced by these species for the following reasons: (1) in a recent experiment, we investigated the potential presence of a scattering signal from solvated electrons in water (see Figure 7 of the Supporting Information). The XDS response of the solvent was very well captured by a model that includes only the heat response, even at excitation intensities up to 26 TW/cm^2, which is almost twice the intensity used in the present experiment. (2) The next prompt photoproduct is the singly ionized $[Fe^{III}(bpy)_3]^{3+}$, which is isoelectronic to the long-lived MLCT state of $[Ru^{III}(bpy)_2(bpy)^{-}]^{2+}$, which we have previously investigated using time-resolved X-ray absorption spectroscopy[54] and femtosecond optical transient absorption spectroscopy.[55] On the basis of this work, we estimate for the oxidized $[Fe^{III}(bpy)_3]^{3+}$ at least a 10-fold smaller structural change (here, shorter Fe−N distance, thus in the other direction) than for the excited HS state structure investigated in the present study. The strong negative feature at low Q in the XDS data indicates that the solute molecules predominantly undergo an expansion; thus we can disregard this product in the current XDS analysis.

Concerning the XES analysis, the solvated electron does not affect it, yet the singly ionized species may contribute to the XES transient (for further details see the Supporting Information). However, in the context of the present analysis, the main use of the XES signal is to determine time zero, and even a possible mixture of HS species with the ionized $[Fe^{III}(bpy)_3]^{3+}$ would not hamper determining time zero, as both are (within the cross correlation time of 0.5 ps) prompt signals.

Due to the presence of excess solvated electrons in the sample, the reduced species $[Fe^{II}(bpy)_3]^{+}$ could also be present. However, this has a formation time of typically a few hundred picoseconds[55] under high fluence conditions; thus it will not contribute to the observed XDS and XES on the 1 ps time scale.

Finally, in a rigorous transient optical absorption study we investigated the occurrence of additional photoproducts in photoexcited aqueous $[Fe^{II}(bpy)_3]^{2+}$ up to 4 TW/cm^2.[28] Interestingly, we always identified the dominant reaction channel GS → MLCT → HS to nearly 100%. Apparently, the efficiency for ionization in a multiphoton process is quite

DOI: 10.1021/acs.jpcb.5b12471
J. Phys. Chem. B 2016, 120, 1158−1168

small, possibly because even high-lying excited states are efficiently funneled into the HS state rather than into a charge transfer to solvent electron ejection process. Furthermore a very recent study by Auböck and Chergui,[11] using femtosecond pump–probe transient absorption spectroscopy in both UV and VIS ranges with sub-60 fs and sub-40 fs time resolutions, respectively, was interpreted as indicating direct population of the HS state in <50 fs concomitant with depopulation of the hot MLCT manifold. These observations further strengthen our conclusions that even at very high excitation intensities, the light-driven formation of HS species is the dominant process for this molecule, leaving practically no pathway for efficient electron ejection from the solute, and therefore the analysis shown here is justified.

3.4. Kinetic Models. Applying the model presented in eq 2 to fit the entire data set with varying time delays −2.5 ps < Δt < 2.5 ps delivered best-fit scaling values for each component in the fit as a function of nominal time delay, and these results are shown in Figure 4 for the three components discussed above.

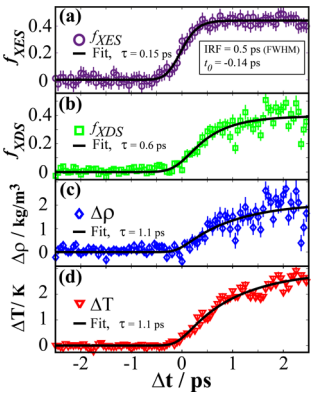

Figure 4. Solute- and solvent-related kinetics data are shown together with best-fit results. Plots in (a) and (b) show the temporal evolution of the fraction of photoexcited solute molecules as determined by XES and XDS, respectively. Black lines show fits of kinetic models (broadened exponential grow in) to the acquired data as described in the main text. The electronic response from the formation of the HS state is observed to precede the structural response, which in turn is faster than the solvent response summarized in (c) and (d).

It is known from previous studies that the photoexcited aqueous $[Fe(bpy)_3]^{2+}$ evolves from the excited MLCT manifold on <30 fs,[18] and its arrival into the ^5T can be described by 150 fs single exponential function.[29,30] As described above, we here adapted the same kinetic model to fit the XES population curve by broadening this with a Gaussian instrument response function with 0.5 ps fwhm. This allows "locking" the t_0 and IRF parameters in subsequent fits of kinetic models to the data shown in Figure 4. In all cases, the kinetic model chosen was a single-exponential grow-in broadened with the IRF and centered at t_0 but allowing each to vary within the 1σ uncertainty interval of the XES fit. The fit results are summarized in Table 1. While XES and XDS are in good agreement regarding the final value for the HS population $f(t)$, their temporal evolution is different for $\Delta t \leq 1$ ps, where $f_{XDS}(\Delta t)$ shows a notably slower increase. We tentatively interpret this as follows: since $f_{XDS}(\Delta t)$ was determined from $\Delta S_{Sol\text{-}cage}$, which also includes solvation cage contributions, the kinetics of this response would be expected to be slower, as the caging solvent molecules require time to adopt a new equilibrium configuration. Additionally, $\Delta S_{Sol\text{-}cage}$ is calculated without including Debye–Waller factors, and as the HS molecule is vibrationally very hot immediately after photoexcitation, this may lead to an underestimate value of $f_{XDS}(\Delta t)$ at the shortest time scales. The fitted τ = 0.6(2) ps for the rise time of $\Delta S_{Sol\text{-}cage}$ could thus correspond to the vibrational cooling within the HS excited state (including internal vibrational redistribution, IVR, and energy dissipation into the caging solvent). Further work in this regard will be focused at explicitly separating solute and cage responses and on the vibrational cooling of the solute molecule as discussed further below.

The two other contributions $\Delta T(\Delta t)$ and $\Delta\rho(\Delta t)$ yield fit results indicating an even slower rise times for both temperature and density changes of ∼1.1 ps (Table 1). All of these results are discussed in detail below, but briefly, for the changes in scattering arising from temperature changes in the solvent, the 1.1 ps rise time is fully expected, since energy impulsively imparted to the solvent takes close to 1 ps to be redistributed into the low-frequency modes commonly referred to as "heat", e.g., as discussed in detail by Lindner et al.[56]

The experiments presented here are the first measurements carried out at LCLS employing simultaneously two complementary ultrafast X-ray techniques on the subpicosecond time scales to study the solvation dynamics of reacting molecules and thus resolving the initial steps involved in the reorganization of the solvent shell around the solute.

Here we underline the high potential of this novel approach to solute–solvent interactions in liquid-phase photochemical reactions on truly ultrafast timescales. In our case, given that the intramolecular relaxation of the molecule occurs on extremely fast time scales,[31] which commences well below the temporal resolution of the present experiment, we cannot look deeply into the early events. However, using prior knowledge, we succeed in distinguishing the "purely" electronic response of photoexcited solute molecules, as depicted in Figure 4a, from slower solute–solvent interactions in Figure 4b. This is only possible due to the simultaneous recording of both XES and XDS in a single measurement, since the XES allows us to precisely determine t_0 of the experiment.

Along with the $f_{XES}(\Delta t)$ determined by the simultaneous measurement of the XES intensity, Figure 4b–d shows the time evolution of $f_{XDS}(\Delta t)$, $\Delta T(\Delta t)$, and $\Delta\rho(\Delta t)$, as determined from the XDS analysis at each measured time delay. We can clearly resolve the slower rise of the solvent-heating signal, which follows the solute–internal, solute–solvent, and solvent–solvent[56] vibrational couplings, until equilibrium is reached after a few picoseconds. The density signal $\Delta\rho(\Delta t)$ in Figure 4c shows very similar temporal behavior as $\Delta T(\Delta t)$ in Figure 4d, within the experimental signal-to-noise (1.1 ps).

To obtain further insights into our current interpretation, we look into the extracted quantitative values for each component in Figure 4. The XDS analysis provides us with the corresponding density and temperature increases of 2.0 ± 0.2 kg/m^3 and 2.75 ± 0.08 K, respectively, where both quantities show approximately the same rise time of 1.1 ps. The obtained time scale for the solvent response is in good agreement with previous femtosecond- and picosecond-resolved studies of water heating due to ultrafast energy release and subsequent structural response (e.g., refs 57–59). In terms of magnitude, we know that the reaction centers are extremely hot immediately after even the most gentle one-photon excitation process, since more than 2 eV is released into each molecule

DOI: 10.1021/acs.jpcb.5b12471
J. Phys. Chem. B 2016, 120, 1158–1168

itself and subsequently into the solvent. Heat dissipation occurs on a 1 ps time scale[30] into both IVR and the solvent, which rapidly leads to cooling of the solute molecules. The energy released by the ultrafast cascade of intersystem crossings and internal conversion processes that leads to population of the HS state following excitation at 400 nm is approximately 2.6 eV per excited solute.[26] With a photoexcitation fraction of 40% of the 50 mM sample solution (=20 mM of excited species), this would result in a temperature increase by only 1.2 K, somewhat lower than the derived 2.8 K increase from the XDS analysis. The remaining discrepancy of 1.6 K we ascribe to the high laser fluence of the 200 μJ, <50 fs laser pulse. Supporting this assignment is the observation that the quality of the model fits to the XDS data improves markedly when the nonlinear temperature dependence of the scattering signal is included in the analysis. However, as detailed in ref 60, this nonlinear response is only significant for temperature changes exceeding tens of degrees, much more than observed in the present analysis. As detailed in the Supporting Information, this seeming discrepancy is resolved by realizing that the sub-50 fs laser excitation pulses have sufficient peak brightness to induce significant photoionization of water through three-photon absorption processes. As discussed by, for example, Crowell et al.,[61] the nonlinear nature of these processes leads to a highly anisotropic excitation profile for the ionization, with very significant deposition of energy in the ~10−20 μm of the liquid sheet facing the incoming laser pump beam with a concomitant large temperature increase in this region of the sample. However, the XDS probe measures the average along the beam path, thus leading to the ~3 K average temperature increase.

One interesting observation in this analysis concerns the rapid density increase in the solvent-only signal extracted from the present analysis in agreement with our previous picosecond study on the same system.[32] The formation of HS solute molecules is accompanied by a rapid increase in the density of the bulk water solvent. This density increase can be similarly assigned to the reorganization of the caging solvent molecules by expulsion of two water molecules from the expanded HS molecule exactly as predicted from high-level modeling.[34] As Figure 4d shows, the density increases by close to 0.2%, or $\Delta\rho$ = 2 kg/m^3. This increase is approximately 3 times higher than observed in the previous synchrotron experiments and in excellent agreement with the higher HS state concentration in the present experiment (20 mM vs 6−8 mM in ref 32). The time scale for this density increase is ~1.1 ps, which is significantly longer than the 0.5(1) ps time resolution of this experiment. Remarkably, the timescales extracted from XDS for population and density are different and in tentative agreement with the similar time scales observed in a recent MD-based studies of dynamic solvation processes for $[Ru(bpy)_3]^{2+}$ in water.[62]

Concerning the solvent contributions to the measured XDS difference signals, we note that $\Delta S_{\Delta T}$ and $\Delta S_{\Delta\rho}$ have been explicitly determined for ensembles of solvent molecules in thermodynamic *equilibrium*, whereas the probed sample volume is in a distinctly *nonequilibrium* state during the first picoseconds following photoexcitation. Despite this apparent limitation, the changes in XDS that can be, at longer times (>100 ps), explicitly related to changes in temperature and density represent rather fundamental measurements of changes in the *local* structure and packing of the solvent, becoming ensemble-averaged in the present experiment. Interestingly, our current analysis indicates that the derived structural changes of the solvent are quite similar on both the ultrafast (<1 ps) and longer time scales (>100 ps). This observation may indicate that the observed changes in X-ray scattering, at both long and short timescales, are intrinsically related to similar changes in the local structure and packing of the solvent, which at longer time scales may be interpreted in terms of thermodynamical changes in equilibrium. Nevertheless, the present study clearly shows the necessity to go beyond the thermodynamical models to analyze ultrafast XDS signals in order to include explicitly short-lived transition states[63] in coupled solute−solvent interactions, which is a formidable task[3,15] beyond the scope of the present study.

3.5. Single-Shot XDS Analysis. From the results presented above, it is evident that the jitter-dominated temporal broadening limits the possibility for direct observation of the formation of the HS state. For a data set corresponding to a nominal time delay Δt = 100 fs, the timing jitter includes data with an *actual* time delay of several hundred femtoseconds apart, which is the cause for the "temporal smearing" of the observed signals. Thus the bin-averaged data at all early time delays already contain contributions from the solvent heating.

However, the fact that the solvent signal needs 1.1 ps to grow in (Figure 4c) implies the possibility that (on very short time scales around t_0) the $\Delta S_{\text{solute+cage}}$ signal could be singled out in selected single-shot measurements before the contributions from the solvent heating and density signals become dominant. Identifying such single shot patterns at the earliest time delay would permit us to compare these XDS shots with the otherwise modeled solute−solvent structural changes, which went into the analysis. In other words, the existence of early time (<100 fs) single shots would allow us to obtain the solute structural signal from the raw data directly. Its identity to the modeled solute structural signal in the prior analysis would thus underline the validity of the chosen approach.

Given the intense XFEL beam delivered by the LCLS, we exploited the opportunity to record XDS patterns in individual single pump−probe shot events, each for which no jitter-induced time smearing is present, but of course without precise knowledge of the actual pump−probe time delay.

Identifying such difference signals with little or no contribution from changes in the solvent is accomplished by applying the fit approach introduced earlier to the many thousands of individual single-shot difference signals and subsequently identifying the set of ΔS curves where the fit yields ΔT and $\Delta\rho$ essentially zero (below 10% of their final values) but with best-fit value of the photoexcitation fraction $f_{\text{XDS}}(\Delta t)$ larger than 0.05. Figure 5c shows the average of seven difference signals identified by applying this procedure. Compared with difference signals acquired at later time points, the absence of a solvent contribution is evident as is the similarity to the calculated $\Delta S_{\text{Sol-cage}}$ shown in Figure 3. Figure 5a shows for comparison a similar average of seven individual difference signals acquired at 1 ps time delay, and Figure 5b shows the average of the same set of difference signals following subtraction of the contributions from heating and density changes. Qualitatively the features of the solute-only single-shot difference signals at $\Delta t \approx 0$ appear somewhat broader than those observed at 1 ps, as would be expected for an ensemble of vibrationally hot HS molecules.

DOI: 10.1021/acs.jpcb.5b12471
J. Phys. Chem. B 2016, 120, 1158−1168

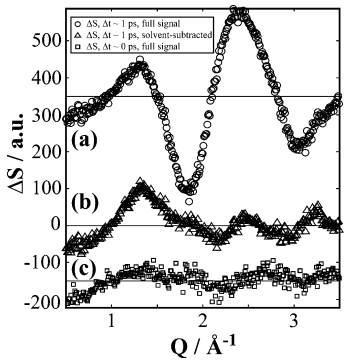

Figure 5. (a) Average of several difference XDS signal (seven pump/probe events) at nominal Δt = 1 ps. (b) Averaged difference signal (black triangles) for the same set of pump/probe events as for (a) but with the solvent contribution subtracted. (c) Average of seven difference signals with essentially no bulk-solvent contribution identified as described in the main text. The solute + cage signals identified at Δt = 1 ps (b) and close to t_0 (c) are similar but not identical.

4. CONCLUSIONS

Overall, the present study reports on the implementation of the complementary techniques of XES and XDS in a single combined pump−probe experiment at the LCLS with subpicosecond time resolution. The goal of this approach is to gain deeper insight into the complex dynamic processes occurring between an impulsively excited solute and its local environment. This delivered new experimental results on the ultrafast events accompanying the solute−solvent interactions occurring nearly concomitant to an ultrafast spin transition process in an aqueous $[Fe(bpy)_3]^{2+}$ complex.

With a probing of both the electronic and structural degrees of freedom simultaneously with subpicosecond time resolution, the information about the structural changes in the solute and the surrounding solvent was obtained by a multicomponent fit to the averaged difference signals. The time resolution of the experiment was governed (and limited) by jitter in the arrival time of the X-ray probe pulses and was approximately 0.5 ps. This time resolution was not sufficient to reveal the fine details of the early electronic structure changes accompanying the spin-state transition.[31] However, the current XDS analysis indicates that the structural rearrangement may complete on a longer time scale than the electronic degrees of freedom. We speculate that the higher than expected value of τ_{HS} determined in the present XDS study (0.6 ± 0.1 ps) compared to the simultaneous as well as previous spectroscopic investigations (0.15 ps) is related to the initially excited molecule being vibrationally hot. The structural models employed in the present study do not incorporate the highly anisotropic structural disorganization associated with a vibrationally hot molecule, and as this would tend to lower the intensity of all features in the difference signals, the derived excitation fraction would be lower in turn. Future work will address this in detail.

On slightly longer time scales the formation of the lowest electronically excited state is observed to be associated with an increase in the density of the solvent, surmised to be associated with the solvent-cage reorganization proposed in ref 34. Significant heating of the solvent was observed to rise within ~1.1 ps. The magnitude of this heating was larger than expected from simple considerations based on energy release from only the photoexcited solute molecules and was concluded to be partly due to direct three-photon ionization of the water molecules. From the volume-averaged temperature increase of 1.5 K ascribed to the three-photon absorption processes and conservatively assuming 1 eV excess energy of the electrons after photoionization in analogy with Crowell et al.,[61] the concentration of solvated electrons is estimated to be in the range of several tens of mM, in agreement with the reported concentrations of solvated electrons $[e^-]$ = 15 mM at significantly lower laser intensity. We note that the presence of a significant concentration of solvated electrons may influence the difference scattering signals, and therefore a more detailed, structural analysis of the acquired difference signals was not attempted, although such an analysis may eventually shed further light on the details of the solvent-cage dynamics.

In an effort to probe the structural response of the sample at very short time scales, a multicomponent fit approach was applied to difference signals arising from single pump−probe shots from the LCLS machine. This was possible because of the very high intensity of the individual X-ray pulses and allowed the identification of those difference signals with essentially no bulk-solvent component. This indicates that even though the reorganization of the solvent shell that manifests itself as a density increase of the bulk solvent is very fast (1.1 ps), the formation of the HS structure does occur first (0.15 ps). The slight differences between the short- and long-delay solute-only difference signals (with the latter being somewhat narrower) are tentatively assigned to the molecules being vibrationally hot immediately after photoexcitation. The ability to measure solute-only signals at very short time delays also shows that it is possible to conduct such pump−probe measurements on timescales short enough for the measured signals to be essentially free from any heat contributions.

The approach used here to identify the structural signals corresponding to the very shortest time delays between the pump and probe pulses relies on the feasibility of applying a model-fit to single difference scattering signals recorded from individual X-ray probe pulses. That this is indeed possible, and also for a molecule comprising mostly light elements, underscores the potential of the new XFELs with 10^{12} photons/pulse as powerful tools for studying fundamental chemical reactions in solution. In particular, the recent implementation of pulse-to-pulse time delay diagnostics with 10 fs time resolution[43,64] offers exciting new opportunities for combined studies of the type presented here to unravel the interplay between electronic structure and molecular geometry in unprecedented detail.

■ ASSOCIATED CONTENT

Supporting Information

The Supporting Information is available free of charge on the ACS Publications website at DOI: 10.1021/acs.jpcb.5b12471.

Additional details concerning data reduction, background subtraction, the solvent response at ultrafast time scales, and second order contributions from bulk solvent heating (PDF)

■ AUTHOR INFORMATION

Corresponding Author

*E-mail: wojciech.gawelda@xfel.eu

Present Addresses

¶A.B.: ICMMO, Université Paris-Sud, UMR CNRS 8182, 15 Avenue Georges Clémenceau, 91405 Orsay Cedex, France.

DOI: 10.1021/acs.jpcb.5b12471
J. Phys. Chem. B 2016, 120, 1158−1168

[∞]M.C.: Institut de Physique de Rennes, UMR UR1-CNRS 6251, Université de Rennes 1, F35042, Rennes, France.

Notes

The authors declare no competing financial interest.

■ ACKNOWLEDGMENTS

This research was funded by the Deutsche Forschungsgemeinschaft (via SFB925, TPA4), by the European XFEL, the Danish National Research Foundations Centre for Molecular Movies, DANSCATT, the Lendület Programme of the Hungarian Academy of Sciences, The Swedish Energy Agency (STEM), the Swedish Research Council, the Knut & Alice Wallenberg Foundation, and the Swiss NNCR-MUST. C.B. acknowledges funding from the Hamburg Center for Ultrafast Imaging (University of Hamburg), G.V. and V.S. acknowledge the European Research Council for Grants ERC-StG-259709 and ERC-AdvG-VISCHEM-226136, respectively, and K.H. gratefully acknowledges funding from the Carlsberg and Villum Foundations. Portions of this research were carried out at the LCLS at SLAC National Accelerator Laboratory. LCLS is an Office of Science User Facility operated for the U.S. Department of Energy Office of Science by Stanford University.

■ REFERENCES

(1) Nitzan, A. *Chemical Dynamics in Condensed Phases: Relaxation, Transfer and Reactions in Condensed Molecular Systems*; Oxford University Press, Oxford, U.K., 2006.
(2) Bressler, C.; Chergui, M. Ultrafast X-Ray Absorption Spectroscopy. *Chem. Rev.* **2004**, *104*, 1781−1812.
(3) Lee, J. H.; Wulff, M.; Bratos, S.; Petersen, J.; Guerin, L.; Leicknam, J.-C.; Cammarata, M.; Kong, Q.; Kim, J.; Møller, K. B.; et al. Filming the Birth of Molecules and Accompanying Solvent Rearrangement. *J. Am. Chem. Soc.* **2013**, *135*, 3255−3261.
(4) Owrutsky, J. C.; Raftery, D.; Hochstrasser, R. M. Vibrational Relaxation Dynamics in Solutions. *Annu. Rev. Phys. Chem.* **1994**, *45*, 519−555.
(5) Greaves, S. J.; Rose, R. A.; Oliver, T. A. A.; Glowacki, D. R.; Ashfold, M. N. R.; Harvey, J. N.; Clark, I. P.; Greetham, G. M.; Parker, A. W.; Towrie, M.; et al. Vibrationally Quantum-State-Specific Reaction Dynamics of H Atom Abstraction by CN Radical in Solution. *Science* **2011**, *331*, 1423−1426.
(6) Rosenthal, S. J.; Xie, X.; Du, M.; Fleming, G. R. Femtosecond Solvation Dynamics in Acetonitrile: Observation of the Inertial Contribution to the Solvent Response. *J. Chem. Phys.* **1991**, *95*, 4715−4718.
(7) Jimenez, R.; Fleming, G. R.; Kumar, P. V.; Maroncelli, M. Femtosecond Solvation Dynamics of Water. *Nature* **1994**, *369*, 471−473.
(8) Gustavsson, T.; Baldacchino, G.; Mialocq, J. C. A Femtosecond Fluorescence Up-Conversion Study of the Dynamic Stokes Shift of the DCM Dye Molecule in Polar and Non-Polar Solvents. *Chem. Phys. Lett.* **1995**, *236*, 587−594.
(9) de Boeij, W. P.; Pshenichnikov, M. S. Ultrafast Solvation Dynamics Explored by Femtosecond Photon Echo Spectroscopies. *Annu. Rev. Phys. Chem.* **1998**, *49*, 99−123.
(10) Oskouei, A. A.; Bräm, O.; Cannizzo, A.; van Mourik, F.; Tortschanoff, A.; Chergui, M. Ultrafast UV Photon Echo Peak Shift and Fluorescence Up Conversion Studies of Non-Polar Solvation Dynamics. *Chem. Phys.* **2008**, *350*, 104−110.
(11) Auboeck, G.; Chergui, M. Sub-50-fs Photoinduced Spin Crossover in [Fe(bpy)3]2+. *Nat. Chem.* **2015**, *7*, 629−633.
(12) Ladanyi, B. M.; Maroncelli, M. Mechanisms of Solvation Dynamics of Polyatomic Solutes in Polar and Nondipolar Solvents: a Simulation Study. *J. Chem. Phys.* **1998**, *109*, 3204−3220.
(13) Dang, L. X.; Rice, J. E.; Caldwell, J.; Kollman, P. A. Ion Solvation in Polarizable Water - Molecular-Dynamics Simulations. *J. Am. Chem. Soc.* **1991**, *113*, 2481−2486.
(14) Karplus, M.; Petsko, G. A. Molecular Dynamics Simulations in Biology. *Nature* **1990**, *347*, 631−639.
(15) Dohn, A. O.; Jónsson, E. Ö.; Kjær, K. S.; van Driel, T. B.; Nielsen, M. M.; Jacobsen, K. W.; Henriksen, N. E.; Møller, K. B. Direct Dynamics Studies of a Binuclear Metal Complex in Solution: the Interplay Between Vibrational Relaxation, Coherence, and Solvent Effects. *J. Phys. Chem. Lett.* **2014**, *5*, 2414−2418.
(16) Bressler, C.; Chergui, M. Molecular Structural Dynamics Probed by Ultrafast X-Ray Absorption Spectroscopy. *Annu. Rev. Phys. Chem.* **2010**, *61*, 263−282.
(17) Canton, S. E.; Zhang, X.; Zhang, J.; van Driel, T. B.; Kjaer, K. S.; Haldrup, K.; Chabera, P.; Harlang, T.; Suarez-Alcantara, K.; Liu, Y.; et al. Toward Highlighting the Ultrafast Electron Transfer Dynamics at the Optically Dark Sites of Photocatalysts. *J. Phys. Chem. Lett.* **2013**, *4*, 1972−1976.
(18) Gawelda, W.; Cannizzo, A.; Pham, V.-T.; van Mourik, F.; Bressler, C.; Chergui, M. Ultrafast Nonadiabatic Dynamics of [FeII(bpy)3] 2+ in Solution. *J. Am. Chem. Soc.* **2007**, *129*, 8199−8206.
(19) Cannizzo, A.; van Mourik, F.; Gawelda, W.; Zgrablic, G.; Bressler, C.; Chergui, M. Broadband Femtosecond Fluorescence Spectroscopy of [Ru(bpy)3]2+. *Angew. Chem.* **2006**, *118*, 3246−3248.
(20) Hedley, G. J.; Ruseckas, A.; Samuel, I. D. W. Ultrafast Intersystem Crossing in a Red Phosphorescent Iridium Complex. *J. Phys. Chem. A* **2009**, *113*, 2−4.
(21) Tang, K.-C.; Liu, K. L.; Chen, I.-C. Rapid Intersystem Crossing in Highly Phosphorescent Iridium Complexes. *Chem. Phys. Lett.* **2004**, *386*, 437−441.
(22) Moret, M.-E.; Tavernelli, I.; Chergui, M.; Rothlisberger, U. Electron Localization Dynamics in the Triplet Excited State of [Ru(bpy)3]2+ in Aqueous Solution. *Chem. - Eur. J.* **2010**, *16*, 5889−5894.
(23) Yeh, A. T.; Shank, C. V.; McCusker, J. K. Ultrafast Electron Localization Dynamics Following Photoinduced Charge Transfer. *Science* **2000**, *289*, 935−938.
(24) Wallin, S.; Davidsson, J.; Modin, J.; Hammarström, L. Femtosecond Transient Absorption Anisotropy Study on [Ru(bpy)3]2+ and [Ru(bpy)(py)4]2+. Ultrafast Interligand Randomization of the MLCT State. *J. Phys. Chem. A* **2005**, *109*, 4697−4704.
(25) Bach, U.; Lupo, D.; Comte, P.; Moser, J. E.; Weissörtel, F.; Salbeck, J.; Spreitzer, H.; Grätzel, M. Solid-State Dye-Sensitized Mesoporous TiO2 Solar Cells with High Photon-to-Electron Conversion Efficiencies. *Nature* **1998**, *395*, 583−585.
(26) Sousa, C.; de Graaf, C.; Rudavskyi, A.; Broer, R.; Tatchen, J.; Etinski, M.; Marian, C. M. Ultrafast Deactivation Mechanism of the Excited Singlet in the Light-Induced Spin Crossover of [Fe(2,2′-Bipyridine)3]2+. *Chem. - Eur. J.* **2013**, *19*, 17541−17551.
(27) Gawelda, W.; Bressler, C.; Saes, M.; Kaiser, M.; Tarnovsky, A. N.; Grolimund, D.; Johnson, S. L.; Abela, R.; Chergui, M. Picosecond Time-Resolved X-Ray Absorption Spectroscopy of Solvated Organometallic Complexes. *Phys. Scr.* **2005**, *T115*, 102−106.
(28) Gawelda, W. Time-Resolved X-ray Absorption Spectroscopy of Transition Metal Complexes. Ph.D. Thesis No. 3673, École Polytechnique Fédérale de Lausanne, Switzerland, 2006; DOI: 10.5075/epfl-thesis-3673.
(29) Bressler, C.; Milne, C.; Pham, V. T.; El Nahhas, A.; van der Veen, R. M.; Gawelda, W.; Johnson, S.; Beaud, P.; Grolimund, D.; Kaiser, M.; et al. Femtosecond XANES Study of the Light-Induced Spin Crossover Dynamics in an Iron(II) Complex. *Science* **2009**, *323*, 489−492.
(30) Consani, C.; Prémont-Schwarz, M.; El Nahhas, A.; Bressler, C.; van Mourik, F.; Cannizzo, A.; Chergui, M. Vibrational Coherences and Relaxation in the High-Spin State of Aqueous [FeII(bpy) 3]2+. *Angew. Chem., Int. Ed.* **2009**, *48*, 7184−7187.
(31) Zhang, W.; Alonso-Mori, R.; Bergmann, U.; Bressler, C.; Chollet, M.; Galler, A.; Gawelda, W.; Hadt, R. G.; Hartsock, R. W.;

DOI: 10.1021/acs.jpcb.5b12471
J. Phys. Chem. B 2016, 120, 1158−1168

Kroll, T.; et al. Tracking Excited-State Charge and Spin Dynamics in Iron Coordination Complexes. *Nature* **2014**, *509*, 345−348.
(32) Haldrup, K.; Vankó, G.; Gawelda, W.; Galler, A.; Doumy, G.; March, A. M.; Kanter, E. P.; Bordage, A.; Dohn, A.; van Driel, T. B.; et al. Guest−Host Interactions Investigated by Time-Resolved X-Ray Spectroscopies and Scattering at MHz Rates: Solvation Dynamics and Photoinduced Spin Transition in Aqueous [Fe(bpy)3]2+. *J. Phys. Chem. A* **2012**, *116*, 9878−9887.
(33) Bressler, C.; Gawelda, W.; Galler, A.; Nielsen, M. M.; Sundström, V.; Doumy, G.; March, A. M.; Southworth, S. H.; Young, L.; Vankó, G. Solvation Dynamics Monitored by Combined X-Ray Spectroscopies and Scattering: Photoinduced Spin Transition in Aqueous [Fe(bpy)3]2+. *Faraday Discuss.* **2014**, *171*, 169−178.
(34) Lawson Daku, L. M.; Hauser, A. Ab Initio Molecular Dynamics Study of an Aqueous Solution of [Fe(bpy)3](Cl)2 in the Low-Spin and in the High-Spin States. *J. Phys. Chem. Lett.* **2010**, *1*, 1830−1835.
(35) Kern, J.; Alonso-Mori, R.; Tran, R.; Hattne, J.; Gildea, R. J.; Echols, N.; Glockner, C.; Hellmich, J.; Laksmono, H.; Sierra, R. G.; et al. Simultaneous Femtosecond X-Ray Spectroscopy and Diffraction of Photosystem II at Room Temperature. *Science* **2013**, *340*, 491−495.
(36) Kern, J.; Tran, R.; Alonso-Mori, R.; Koroidov, S.; Echols, N.; Hattne, J.; Ibrahim, M.; Gul, S.; Laksmono, H.; Sierra, R. G.; et al. Taking Snapshots of Photosynthetic Water Oxidation Using Femtosecond X-ray Diffraction and Spectroscopy. *Nat. Commun.* **2014**, *5* (4371), 1−11.
(37) Arnlund, D.; Johansson, L. C.; Wickstrand, C.; Barty, A.; Williams, G. J.; Malmerberg, E.; Davidsson, J.; Milathianaki, D.; DePonte, D. P.; Shoeman, R. L.; et al. Visualizing a Protein Quake with Time-Resolved X-Ray Scattering at a Free-Electron Laser. *Nat. Methods* **2014**, *11*, 923−926.
(38) Levantino, M.; Schiró, G.; Lemke, H. T.; Cottone, G.; Glownia, J. M.; Zhu, D.; Chollet, M.; Ihee, H.; Cupane, A.; Cammarata, M. Ultrafast Myoglobin Structural Dynamics Observed with an X-Ray Free-Electron Laser. *Nat. Commun.* **2015**, *6*, 6772.
(39) Canton, S. E.; Kjaer, K. S.; Vankó, G.; van Driel, T. B.; Adachi, S.-I.; Bordage, A.; Bressler, C.; Chabera, P.; Christensen, M.; Dohn, A. O.; et al. Visualizing the Non-Equilibrium Dynamics of Photoinduced Intramolecular Electron Transfer with Femtosecond X-ray Pulses. *Nat. Commun.* **2015**, *6*, 6359.
(40) Emma, P.; Akre, R.; Arthur, J.; Bionta, R.; Bostedt, C.; Bozek, J.; Brachmann, A.; Bucksbaum, P.; Coffee, R.; Decker, F. J.; et al. First Lasing and Operation Ångström-Wavelength Free-Electron Laser. *Nat. Photonics* **2010**, *4*, 641−647.
(41) Lemke, H. T.; Bressler, C.; Chen, L. X.; Fritz, D. M.; Gaffney, K. J.; Galler, A.; Gawelda, W.; Haldrup, K.; Hartsock, R. W.; Ihee, H.; et al. Femtosecond X-Ray Absorption Spectroscopy at a Hard X-Ray Free Electron Laser: Application to Spin Crossover Dynamics. *J. Phys. Chem. A* **2013**, *117*, 735−740.
(42) Hart, P.; Boutet, S.; Carini, G.; Dubrovin, M.; Duda, B.; Fritz, D.; Haller, G.; Herbst, R.; Herrmann, S.; Kenney, C.; et al. The Cornell-SLAC Pixel Array Detector at LCLS. *Proc. SPIE* **2012**, *85040C*, 538−541.
(43) Harmand, M.; Coffee, R.; Bionta, M. R.; Chollet, M.; French, D.; Zhu, D.; Fritz, D. M.; Lemke, H. T.; Medvedev, N.; Ziaja, B.; et al. Achieving Few-Femtosecond Time-Sorting at Hard X-Ray Free-Electron Lasers. *Nat. Photonics* **2013**, *7*, 215−218.
(44) Vankó, G.; Neisius, T.; Molnár, G.; Renz, F.; Kárpáti, S.; Shukla, A.; de Groot, F. M. F. Probing the 3d Spin Momentum with X-Ray Emission Spectroscopy: the Case of Molecular-Spin Transitions. *J. Phys. Chem. B* **2006**, *110*, 11647−11653.
(45) Vankó, G.; Bordage, A.; Glatzel, P.; Gallo, E.; Rovezzi, M.; Gawelda, W.; Galler, A.; Bressler, C.; Doumy, G.; March, A. M.; et al. *J. Electron Spectrosc. Relat. Phenom.* **2013**, *188*, 166−171.
(46) Haldrup, K.; Christensen, M.; Meedom Nielsen, M. Analysis of Time-Resolved X-Ray Scattering Data From Solution-State Systems. *Acta Crystallogr., Sect. A: Found. Crystallogr.* **2010**, *66*, 261−269.
(47) Haldrup, K. Singular Value Decomposition as a Tool for Background Corrections in Time-Resolved XFEL Scattering Data. *Philos. Trans. R. Soc., B* **2014**, *369*, 20130336.
(48) Kong, Q.; Kjaer, K. S.; Haldrup, K.; Sauer, S. P. A.; van Driel, T. B.; Christensen, M.; Nielsen, M. M.; Wulff, M. Theoretical Study of the Triplet Excited State of PtPOP and the Exciplexes M-PtPOP (M = Tl, Ag) in Solution and Comparison with Ultrafast X-ray Scattering Results. *Chem. Phys.* **2012**, *393*, 117−122.
(49) Kong, Q.; Lee, J. H.; Plech, A.; Wulff, M.; Ihee, H.; Koch, M. H. J. Ultrafast X-Ray Solution Scattering Reveals an Unknown Reaction Intermediate in the Photolysis of [Ru3(CO)12]. *Angew. Chem., Int. Ed.* **2008**, *47*, 5550−5553.
(50) Jun, S.; Lee, J. H.; Kim, J.; Kim, J.; Kim, K. H.; Kong, Q.; Kim, T. K.; Lo Russo, M.; Wulff, M.; Ihee, H. Photochemistry of HgBr2 in Methanol Investigated Using Time-Resolved X-Ray Liquidography. *Phys. Chem. Chem. Phys.* **2010**, *12*, 11536−11547.
(51) Gawelda, W.; Pham, V.-T.; Benfatto, M.; Zaushitsyn, Y.; Kaiser, M.; Grolimund, D.; Johnson, S. L.; Abela, R.; Hauser, A.; Bressler, C.; et al. Structural Determination of a Short-Lived Excited Iron(II) Complex by Picosecond X-ray Absorption Spectroscopy. *Phys. Rev. Lett.* **2007**, *98*, 057401.
(52) Cammarata, M.; Lorenc, M.; Kim, T. K.; Lee, J. H.; Kong, Q. Y.; Pontecorvo, E.; Lo Russo, M.; Schiró, G.; Cupane, A.; Wulff, M.; et al. Impulsive Solvent Heating Probed by Picosecond X-Ray Diffraction. *J. Chem. Phys.* **2006**, *124*, 124504.
(53) Kjær, K. S.; van Driel, T. B.; Kehres, J.; Haldrup, K.; Khakhulin, D.; Bechgaard, K.; Cammarata, M.; Wulff, M.; Sørensen, T. J.; Nielsen, M. M. Introducing a Standard Method for Experimental Determination of the Solvent Response in Laser Pump, X-Ray Probe Time-Resolved Wide-Angle X-Ray Scattering Experiments on Systems in Solution. *Phys. Chem. Chem. Phys.* **2013**, *15*, 15003−15016.
(54) Gawelda, W.; Johnson, M.; de Groot, F. M. F.; Abela, R.; Bressler, C.; Chergui, M. Electronic and Molecular Structure of Photoexcited [RuII(bpy)3]2+ Probed by Picosecond X-Ray Absorption Spectroscopy. *J. Am. Chem. Soc.* **2006**, *128*, 5001−5009.
(55) Tarnovsky, A. N.; Gawelda, W.; Johnson, M.; Bressler, C.; Chergui, M. Photexcitation of Aqueous Ruthenium(II)-Tris-(2,2′-Bipyridine) with High-Intensity Femtosecond Laser Pulses. *J. Phys. Chem. B* **2006**, *110*, 26497−26505.
(56) Lindner, J.; Vöhringer, P.; Pshenichnikov, M. S.; Cringus, D.; Wiersma, D. A.; Mostovoy, M. Vibrational Relaxation of Pure Liquid Water. *Chem. Phys. Lett.* **2006**, *421*, 329−333.
(57) Wen, H.; Huse, N.; Schoenlein, R. W.; Lindenberg, A. M. Ultrafast Conversions Between Hydrogen Bonded Structures in Liquid Water Observed by Femtosecond X-ray Spectroscopy. *J. Chem. Phys.* **2009**, *131*, 234505.
(58) Ashihara, S.; Huse, N.; Espagne, A.; Nibbering, E. T. J.; Elsaesser, T. Ultrafast Structural Dynamics of Water Induced by Dissipation of Vibrational Energy. *J. Phys. Chem. A* **2007**, *111*, 743−746.
(59) Madsen, D.; Thomsen, C. L.; Thøgersen, J.; Keiding, S. R. Temperature Dependent Relaxation and Recombination Dynamics of the Hydrated Electron. *J. Chem. Phys.* **2000**, *113*, 1126−1134.
(60) Neuefeind, J.; Benmore, C. J.; Weber, J. K. R.; Paschek, D. More Accurate X-Ray Scattering Data of Deeply Supercooled Bulk Liquid Water. *Mol. Phys.* **2011**, *109*, 279−288.
(61) Crowell, R. A.; Lian, R.; Shkrob, I. A.; Qian, J.; Oulianov, D. A.; Pommeret, S. Light-Induced Temperature Jump Causes Power-Dependent Ultrafast Kinetics of Electrons Generated in Multiphoton Ionization of Liquid Water. *J. Phys. Chem. A* **2004**, *108*, 9105−9114.
(62) Szymczak, J. J.; Hofmann, F. D.; Meuwly, M. Structure and Dynamics of Solvent Shells Around Photoexcited Metal Complexes. *Phys. Chem. Chem. Phys.* **2013**, *15*, 6268−6277.
(63) Møller, K. B.; Henriksen, N. E. Time-Resolved X-Ray Diffraction: the Dynamics of the Chemical Bond. *Struct. Bonding (Berlin, Ger.)* **2011**, *142*, 185−211.
(64) Bionta, M. R.; Lemke, H. T.; Cryan, J. P.; Glownia, J. M.; Bostedt, C.; Cammarata, M.; Castagna, J.-C.; Ding, Y.; Fritz, D. M.; Fry, A. R.; et al. Spectral Encoding of X-Ray/Optical Relative Delay. *Opt. Express* **2011**, *19*, 21855−21865.

DOI: 10.1021/acs.jpcb.5b12471
J. Phys. Chem. B 2016, 120, 1158−1168

(65) Das, A. K.; Solomon, R. V.; Hofmann, F.; Meuwly, M. Inner-Shell Water Rearrangement Following Photoexcitation of Tris(2,2′-bipyridine)iron(II). *J. Phys. Chem. B* **2016**, *120*, 206−216.

NOTE ADDED IN PROOF

Following submission of the present manuscript, the existence of the recently published article "Inner-Shell Water Rearrangement Following Photoexcitation of Tris(2,2′-bipyridine)iron(II)" by A. K. Das et al.[65] has come to our attention. We note that the time scale found for the ultrafast density increase reported in our present paper is in good agreement with the simulation results of Das et al. We would, however, like to emphasize that our previously published results on the solvation response upon the LS → HS transition in $Fe(bpy)_3$[32] only reports 100 ps as the time resolution of the (synchrotron-based) experiment, not as the time scale of exchange dynamics, as claimed in article by Das et al.

DOI: 10.1021/acs.jpcb.5b12471
J. Phys. Chem. B 2016, 120, 1158−1168